Available online at www.sciencedirect.com
SCIENCE DIRECT®
Journal of Nuclear Materials 340 (2005) 237–246
journal of nuclear materials
www.elsevier.com/locate/jnucmat

Corrosion behavior of Zr alloys with a high Nb content

Jeong-Yong Park *, Byung-Kwon Choi, Yong Hwan Jeong, Youn-Ho Jung

Zirconium Fuel Cladding Team, Korea Atomic Energy Research Institute, 150 Deokjin-dong, Yuseong-gu, Daejeon 305-353, Republic of Korea

Received 6 May 2004; accepted 1 December 2004

Abstract

The corrosion behavior of the Zr alloy with a high Nb content was evaluated in the water loop system containing 2.2 wppm Li and 650 wppm B. The characteristics of the precipitates were analyzed by transmission electron microscopy (TEM) and the oxide was characterized by an X-ray diffraction method using a synchrotron radiation source. On the basis of the results obtained by these measurements, the relationship among the oxidation behavior, the precipitate characteristics and the oxide properties was discussed. It was shown that the Cu addition was of benefit to the corrosion resistance of the Zr alloy with a high Nb content and the corrosion resistance of the Cu-containing alloy (Zr–1.5Nb–0.5Sn–0.2Fe–0.1Cu) was superior to that of the Cr-containing alloy (Zr–1.5Nb–0.5Sn–0.2Fe–0.1Cr). The fine β-Nb precipitates were found more frequently in the Cu-containing alloy than the Cr-containing alloy when heat-treated in the same condition. The fraction of the tetragonal zirconia in the region of the metal/oxide interface was higher in the Cu-containing alloy than the Cr-containing alloy, suggesting that the stabilization of the tetragonal phase in the oxide was promoted more when the smaller precipitates are incorporated into the oxide. It is concluded that the fine distribution of β-Nb is desirable for stabilizing the tetragonal phase in the oxide, thereby increasing the corrosion resistance of the Zr alloy with a high Nb content.

PACS: 81.65.K; 81.65.M; 29.20.L

1. Introduction

A development of more corrosion resistant Zr alloys than Zircaloy-4 has been required by the current more demanding operation conditions and discharge burnups in the pressurized water reactor (PWR) [1]. A number of recent works concentrated on the development of new Zr alloys have shown that Nb would be the most beneficial alloying element to improve the corrosion resistance of Zr alloys [2–6]. Although many studies [2–6] were conducted to evaluate the corrosion behavior of Nb-containing Zr alloys in out-of-pile and in-pile conditions, the optimum Nb content for the corrosion performance was changed according to the chemical compositions and manufacturing processes.

Among the metallurgical parameters which are determined by the manufacturing process, the precipitates are known to play a critical role in influencing the corrosion resistance. The precipitates are incorporated into the oxide film in unoxidized state because the oxidation of the intermetallic precipitates is delayed compared to

* Corresponding author. Tel.: +82 42 868 8911; fax: +82 42 862 0432.
E-mail address: parkjy@kaeri.re.kr (J.-Y. Park).

0022-3115/$ - see front matter © 2005 Elsevier B.V. All rights reserved.
doi:10.1016/j.jnucmat.2004.12.003

the Zr matrix. The late oxidation of the incorporated precipitates is accompanied by a change of the oxide properties. A number of works revealed that the corrosion resistance of Zr alloys was highly dependent on the particle size distribution of the precipitate [4,6–8]. However, the effect of the precipitate size on the corrosion resistance of Nb-containing Zr alloys [4,6,7] was contrary to that of Zircaloy-4 [8,9]. Therefore, in order to improve the corrosion resistance of Nb-containing Zr alloys, it is essential to examine the effect of the precipitate characteristics on the corrosion behavior of Nb-containing Zr alloys.

In the authors' previous study [10], the Zr alloy with a high Nb content (1.5 wt% Nb) showed an excellent corrosion resistance as compared to the Zr alloy with a low Nb content (0.4 wt% Nb) when properly heat-treated to obtain the metallurgical structure in which the fine precipitates were homogeneously distributed. This result has led to additional studies on the oxidation mechanisms of Zr alloys with a high Nb content in order to better understand the effects of the metallurgical state and the chemical composition on the corrosion mechanisms [11,12]. The preliminary results made it possible to consider the Zr alloy with a high Nb content as one of the most promising alloys as a substitute for Zircaloy-4.

The aim of this study is to investigate the corrosion behavior of Zr alloys with a high Nb content in a condition simulating the water chemistry of PWRs. The characteristics of the precipitates were analyzed by transmission electron microscopy (TEM) and the oxide was characterized by an X-ray diffraction method using synchrotron radiation. On the basis of the results obtained by these measurements, the relationship among the corrosion behavior, the precipitate characteristics and the oxide properties was discussed.

2. Experimental methods

The chemical compositions of the Zr alloys used in this study are shown in Table 1. Button ingots of approximately 200 g were prepared by arc melting under an argon atmosphere and remelted at least five times to promote the homogeneity of the as-cast structure. The arc-melted ingots were β-solution treated at 1020 °C for 30 min in a vacuum furnace, hot-rolled after preheating to 610 °C for 10 min and cold-rolled three times to a final thickness of 1 mm. Between the rolling steps, the cold-rolled sheets were intermediate-annealed at 575 °C for 3 h to obtain the fully-recrystallized structure. Especially, at the annealing step after hot rolling, the variable annealing time ranging from 3 h to 15 h was applied to change the size of the precipitate which is known to play a key roll in controlling the corrosion kinetics of Zr alloys. The final cold-rolled sheets were annealed at 510 °C for 2.5 h to obtain the partially-recrystallized metallurgical form.

Specimens for the corrosion test, 15 by 20 by 1 mm in size, were cut from the partially-recrystallized sheets, mechanically ground by use of 800 grit SiC paper, and then pickled in a solution of 5 vol.% HF, 45 vol.% HNO_3 and 50 vol.% H_2O. The corrosion tests were conducted at 360 °C in the water loop system containing 2.2 wppm Li and 650 wppm B under the pressure of 18.5 MPa in a manner consistent with the ASTM Practice for Aqueous Corrosion Testing of Samples of Zirconium and Zirconium Alloys (G2-88). The corrosion behavior of the specimens was evaluated by measuring the weight gain with the exposure time.

The microstructures of the alloys were examined using a transmission electron microscope (TEM) equipped with an energy dispersive X-ray spectroscope (EDS). Specimens for TEM observation were prepared by a twin-jet polishing with a solution of 10 vol.% $HClO_3$ and 90 vol.% C_2H_5OH after mechanical thinning to 70 μm. It is well known that the corrosion resistance of Zr alloys depends on the characteristics of the precipitates. The microstructure characterization was concentrated on the variation of the precipitation behavior with the alloying elements and heat treatment conditions. The selected area diffraction patterns (SADP) were obtained and analyzed to determine the crystal structure of the precipitates, and the micro-chemical

Table 1
Chemical compositions and heat treatment conditions of the Zr alloys

Specimen ID	Chemical compositions						Annealing condition after hot rolling
	Nb	Sn	Fe	Cr	Cu	Zr	
A	1.5	0.5	0.2			Bal.	575 °C, 8 h
B	1.5	0.5	0.2	0.1		Bal.	575 °C, 8 h
C	1.5	0.5	0.2		0.1	Bal.	575 °C, 3 h
D	1.5	0.5	0.2		0.1	Bal.	575 °C, 8 h
E	1.5	0.5	0.2		0.1	Bal.	575 °C, 15 h
F	1.5	0.5	0.2	0.05	0.05	Bal.	575 °C, 8 h

analyses on the precipitates were conducted using EDS. Particle size distributions were also measured using an image analyzer.

The oxide characterization was carried out by an X-ray diffraction method using synchrotron radiation. The experiment was performed using a standard six-circle diffractometer at the 3C2 bending magnet beamline in the Pohang Light Source (PLS). In order to analyze the crystal structure of the oxide formed at the surface of the specimen, the incident angle of the X-ray was fixed in the range of 0.5° to 3°. Upon varying the incident angle from 0.5° to 3°, it was possible to assess the crystal structure of the oxide as a function of the depth because the penetration depth of the X-ray increased by increasing the incident angle.

3. Results and discussion

3.1. Corrosion behavior

The corrosion behavior of the Zr alloys used in this study is shown in Fig. 1. The corrosion kinetics of the Zr alloys was compared with each other and the influence of the alloying element on the corrosion resistance of Zr–1.5Nb–0.5Sn–0.2Fe was examined. Under the corrosion condition employed in this study, which simulated the water chemistry of PWRs, the Cu-containing alloy showed the best corrosion resistance among the alloys tested. The corrosion resistance of the Cr-containing alloy was lower than that of Zr–1.5Nb–0.5Sn–0.2Fe. The corrosion resistance of the Cr/Cu-containing alloy is comparable to that of Zr–1.5Nb–0.5Sn–0.2Fe, suggesting that the detrimental effect of the Cr addition was compensated for by the beneficial effect of the Cu addition. It was note worthy that the corrosion resistance of the Cu-containing alloy was superior to the Cr-containing alloy and the Cu addition is of benefit to the corrosion resistance of Zr–1.5Nb–0.5Sn–0.2Fe.

Fig. 2 shows the effect of the intermediate annealing time after the hot rolling on the corrosion behavior of the Cu-containing alloy (Zr–1.5Nb–0.5Sn–0.2Fe–0.1Cu) showing the best corrosion resistance among the alloys tested. The three alloys showed almost the same corrosion behavior in the pre-transition regime. After the kinetic transition, however, the corrosion rate of the Cu-containing alloys increased by increasing the intermediate annealing time. Anada et al. reported that the annealing after hot rolling influenced the uniform corrosion more significantly than the other intermediate and final annealings [8]. It was also reported that the intermediate annealing after hot rolling was the most important step to determine the microstructural features, particularly the characteristics of the precipitates [10]. It is therefore possible to consider that the corrosion behavior of the Cu-containing alloy is highly influenced by the precipitate characteristics, which is practically determined by the intermediate annealing after hot rolling.

3.2. Microstructure characterization

The typical microstructures of the alloys were found to be the partially-recrystallized structures consisting mainly of recrystallized grains and a small portion of the cold worked structure with a high density of dislocations. Fig. 3 shows the typical distribution of the precipitates in the recrystallized grain of the alloys. It was shown that the precipitates were randomly distributed within the grains and along the grain boundaries in both

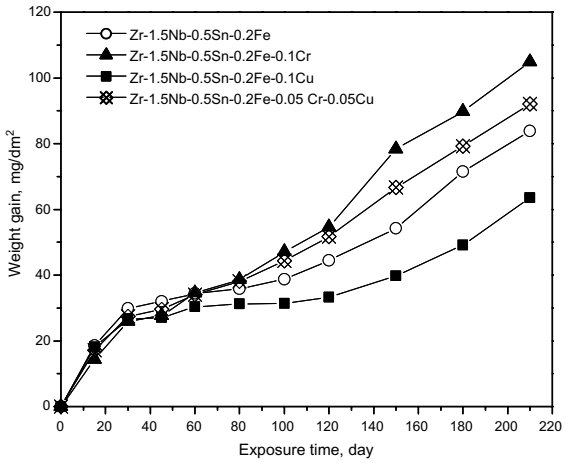

Fig. 1. Effects of Cr and Cu addition on the corrosion behavior of Zr–1.5Nb–0.5Sn–0.2Fe at 360 °C in the water loop containing 2.2 wppm Li and 650 wppm B.

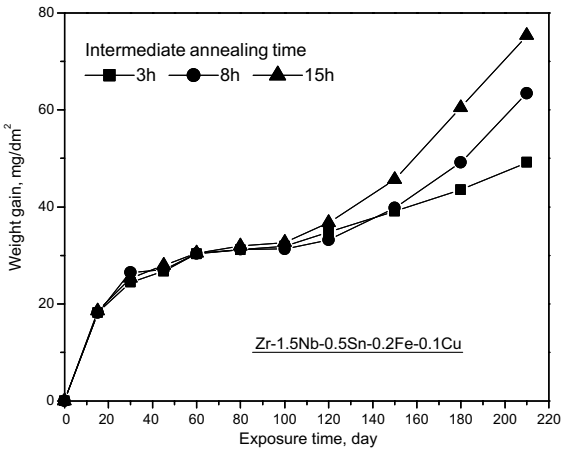

Fig. 2. Effects of the intermediate annealing time after the hot rolling on the corrosion behavior of Zr–1.5Nb–0.5Sn–0.2Fe–0.1Cu at 360 °C in the water loop containing 2.2 wppm Li and 650 wppm B.

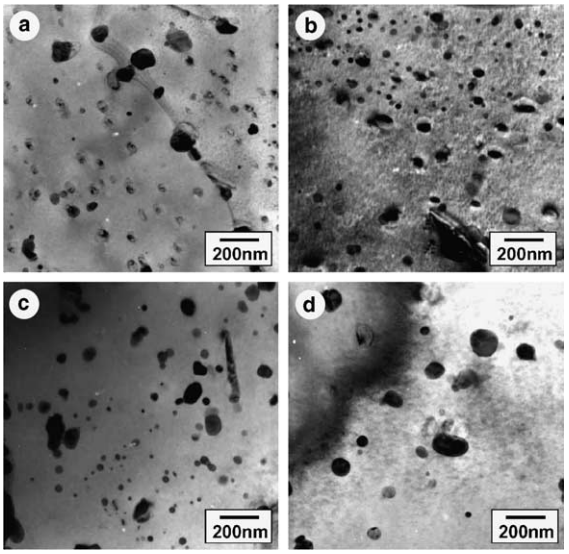

Fig. 3. Transmission electron micrographs of the precipitates in the recrystallized grain of (a) Zr–1.5Nb–0.5Sn–0.2Fe–0.1Cr intermediate-annealed at 575 °C for 8 h and (b,c,d) Zr–1.5Nb–0.5Sn–0.2Fe–0.1Cu intermediate-annealed at 575 °C for (b) 3 h, (c) 8 h and (d) 15 h.

alloys. In the authors' previous study [13] to examine the effect of the final microstructure on the corrosion resistance of Zr alloys with a high Nb content, the best corrosion resistance was obtained in the partially recrytallized structure. However, the difference of the corrosion resistance between the partially-recrystallized structure and the others was very small. It is noted here that the corrosion resistance of the Nb-containing Zr alloys was not seriously affected by the degree of the recrystallization in the final microstructure but markedly dependant on the characteristics of the precipitates.

The crystal structure and the chemical composition of the precipitate were assessed by TEM. In the Cr-containing alloy, the precipitates were identified as β-Nb with a bcc crystal structure and the $Zr(Fe,Cr)_2$-type precipitate containing Nb. The intermetallic $Zr(Fe,Cr)_2$-type precipitate was found to have a C14-type hexagonal structure. Fig. 4 shows the TEM bright field image, dark field image, SADP and the EDS spectrum on the $Zr(Fe,Cr)_2$-type precipitate in the Cr-containing alloy. On the other hand, the precipitates in the Cu-containing alloys were identified as the β-Nb and the Zr_3Fe-type precipitate containing Nb and Cu. The TEM bright field image, dark field image, SADP and the EDS spectrum for the β-Nb in the Cu-containing alloy are depicted in Fig. 5. It was reported that the Zr_2Cu intermetallic compound was precipitated in the Zr–Cu binary alloy [14]. However, Zr_2Cu-type precipitate was not found in the Cu-containing alloy used in this study even though the intermediate annealing time was increased.

3.3. Effects of the precipitates on the corrosion behavior

Hong et al. reported that the optimum Cu concentration for improving the corrosion resistance of the modified Zircaloy-4 was thought to be around 0.1–0.2 wt% [14]. But the effect of a Cu addition on the corrosion behavior was not well established. Moreover, in the Nb-containing Zr alloys, the effect of the Nb was reported to be stronger than that of the other alloying elements such as Fe and Cr [9]. It was reported that the best corrosion performance of the Zr–1Nb–1Sn–0.1Fe alloys was obtained for the microstructure containing β-Nb and the deviation from this microstructure, such as the presence of β-Zr, tended to degrade the corrosion resistance [6,7]. The corrosion resistance of the binary Zr–Nb alloys was improved when the second phase particles were β-Nb with an equilibrium concentration of the Nb in the matrix [15,16]. It was also confirmed that the precipitation of β-Nb enhanced the out-of-pile and in-pile corrosion resistance in the Zr–1.0Nb–0.12O alloys [4]. This seems to be indicative that the precipitation of the second phase particle containing Nb is closely related to the corrosion behavior.

In this study, the exact volume fraction of each type of the precipitate was not calculated because the precise

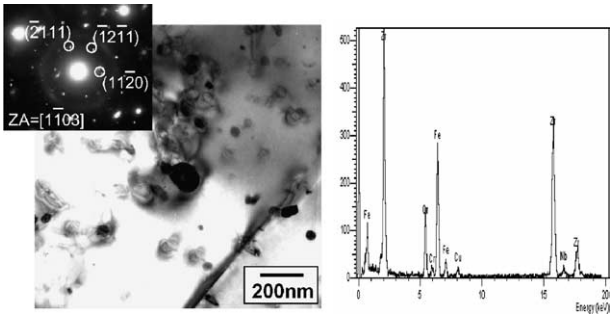

Fig. 4. TEM bright field image, dark field image, selected area diffraction pattern (SADP) and EDS spectrum on $Zr(Fe,Cr)_2$-type precipitate in Cr-containing alloy intermediate-annealed at 575 °C for 8 h.

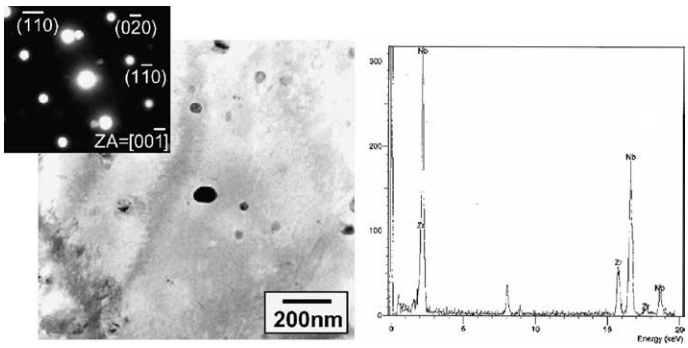

Fig. 5. TEM bright field image, dark field image, selected area diffraction pattern (SADP) and the EDS spectrum on β-Nb precipitate in Cu-containing alloy intermediate-annealed at 575 °C for 8 h.

distinction was not facilitated in the TEM image. But it seems that the fine precipitates were mostly ascertained by β-Nb whereas the relatively large particles were the $Zr(Fe,Cr)_2$-type precipitate in the Cr-containing alloy and the Zr_3Fe-type precipitates in the Cu-containing alloy. And the fine β-Nb precipitates were found more frequently in the Cu-containing alloy than the Cr-containing alloy when heat-treated in the same condition. It is thought that the amount of the precipitate originating from Cu is smaller than that of Cr because the maximum solubility of Cu (0.2 wt%) in α-Zr was larger than that of Cr (0.02 wt%) although the solubility would be much lower at low temperatures. Consequently, the relative fraction of β-Nb is higher in the Cu-containing alloys than the Cr-containing alloy. This seems to be one of the reasons why the corrosion resistance of the Cu-containing alloy is superior to that of the Cr-containing alloys, as shown in Fig. 1.

Fig. 6 shows the typical histograms of the particle size distributions calculated using an image analyzer for the precipitates in the Cr- and Cu-containing alloys. More than three hundred particles were counted to measure the size distribution and the mean particle size. The calculated mean particle sizes are indicated in the Figs. It was found that the mean particle size of the Cu-containing alloy was smaller than that of the Cr-containing alloy when they were intermediate-annealed in the same condition, namely, at 575 °C for 8 h. In the Cu-containing alloy, the mean particle size increased from 49 nm to 94 nm by increasing the intermediate annealing time from 3 h to 15 h.

A number of works revealed that the corrosion resistance of Zr alloys was highly dependent on the particle size distribution of the precipitate [4,6–8]. In the Nb-containing Zr alloys, however, the relationship between the size distribution and the corrosion resistance has not been well established. Moreover, the effect of the precipitate size on the corrosion resistance of the Nb-containing Zr alloys [4,6,7] was contrary to that of Zircaloy-4 [8,9].

The optimum corrosion performance of the Nb-containing Zr alloys was achieved when the fine second phase particles was uniformly precipitated in the matrix [15,16]. It was also reported that the Zr–Nb and Zr–Nb–Sn alloys revealed a good corrosion resistance when the alloy possessed the precipitates with an average particle size of approximately 50 nm by a low-temperature aging following β treatment [17]. When the average particle size was coarsened to 200–300 nm, a significant degradation in the corrosion resistance was observed [17]. These results are consistent with that of the present study and imply that the size of precipitate plays an important role in the corrosion behavior of the Nb-containing Zr alloy and the precipitation of fine precipitates is essential to obtain the optimum microstructure for improving the corrosion resistance.

3.4. Oxide characterization by Synchrotron radiation

The crystal structure of the oxide in the pre-transition regime was examined by a glancing angle X-ray diffraction method using a synchrotron radiation source, in which the incident angle was varied from 0.5° to 3°. As the penetration depth of the X-ray increases with increasing the incident angle, the diffraction volume by the X-ray changes from the outer surface region to the volume covering the surface to the metal/oxide interface [18]. Fig. 7 shows the diffracted intensity (arbitrary unit) at the incident angles of 0.5°, 1°, 2° and 3° measured on the oxide of the Cr-containing alloy corroded up to a weight gain of about 25 mg/dm^2. The same experiment was also performed for the oxide of the Cu-containing alloy corroded up to a weight gain of about 25 mg/dm^2, and the result is depicted in Fig. 8. The X-ray diffraction peaks for the monoclinic and the tetragonal phase were observed, but the relative intensity of the monoclinic or the tetragonal phase changed with the incident angle.

In addition, the diffraction peaks for Zr (0002) and Zr (101) were also observed at an incident angle of 3°.

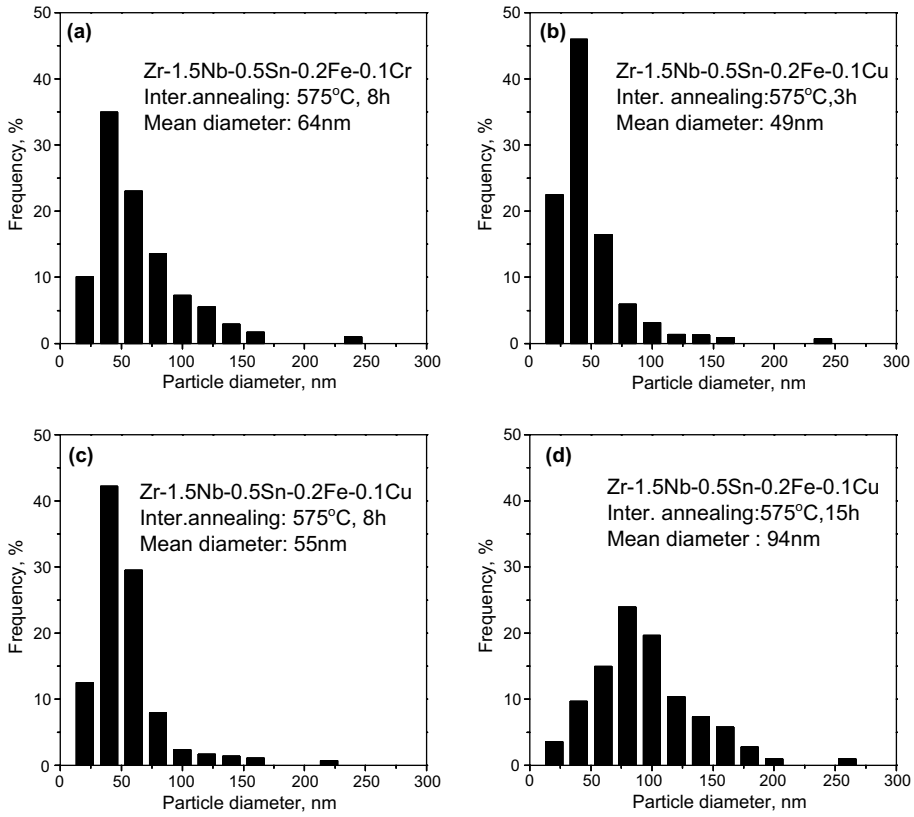

Fig. 6. Histograms of the particle size distribution calculated using an image analyzer for the precipitates in (a) Zr–1.5Nb–0.5Sn–0.2Fe–0.1Cr intermediate-annealed at 575 °C for 8 h and (b,c,d) Zr–1.5Nb–0.5Sn–0.2Fe–0.1Cu intermediate-annealed at 575 °C for (b) 3 h, (c) 8 h and (d) 15 h.

From the XRD results, it was shown that the oxide was the mixture of the tetragonal zirconia and monoclinic one, and the fraction of the tetragonal or the monoclinic zirconia changed with the oxide depth. The synchrotron radiation with a much higher flux density, compared to a conventional X-ray source, made it possible to precisely detect a small amount of the tetragonal zirconia in the oxide layer. Erwin et al. obtained a quantitative measurement of the small volume fractions of the precipitates present in the Zr alloys using the synchrotron X-ray source [19]. However, the exact quantification of the tetragonal zirconia was not carried out in this study. But it was enough to reach a satisfactory elucidation from the preliminary quantification as measured by the synchrotron X-ray diffraction peaks.

From the results of Figs. 7 and 8, the integrated intensities were calculated for the X-ray diffraction peaks of the monoclinic ZrO_2 (11), the monoclinic ZrO_2 (111) and the tetragonal ZrO_2 (101). And the fraction of the tetragonal phase was calculated using the Garvie–Nicholson formula which was proposed to calculate the phase fraction of the ZrO_2 powder [20].

Fig. 9 shows the fraction of the tetragonal phase intensity as a function of the depth from the outer surface to the metal/oxide interface in the Cr- and Cu-containing alloys. It was revealed that the fraction of the tetragonal phase increased with increasing the incident angle, that is, from the outer surface to the metal/oxide interface, both in the Cr- and Cu-containing alloys. The tetragonal zirconia formed in the metal/oxide interface was transformed to the monoclinic zirconia in the kinetic transition. Thus, the fraction of the tetragonal zirconia decreases from the metal/oxide interface to the outer surface as shown in Fig. 9. However, the fraction of the tetragonal phase in the region of the metal/oxide interface was higher in the Cu-containing alloy than the Cr-containing alloy.

Since it is widely known that the oxide formed on the Zr alloys has a texture structure, the texture correction should be performed to obtain the precise calculation of the phase fraction. In this investigation, however, the assumption that the texture does not change greatly with oxide thickness and with alloy type was applied because what was emphasized in this study was the differ-

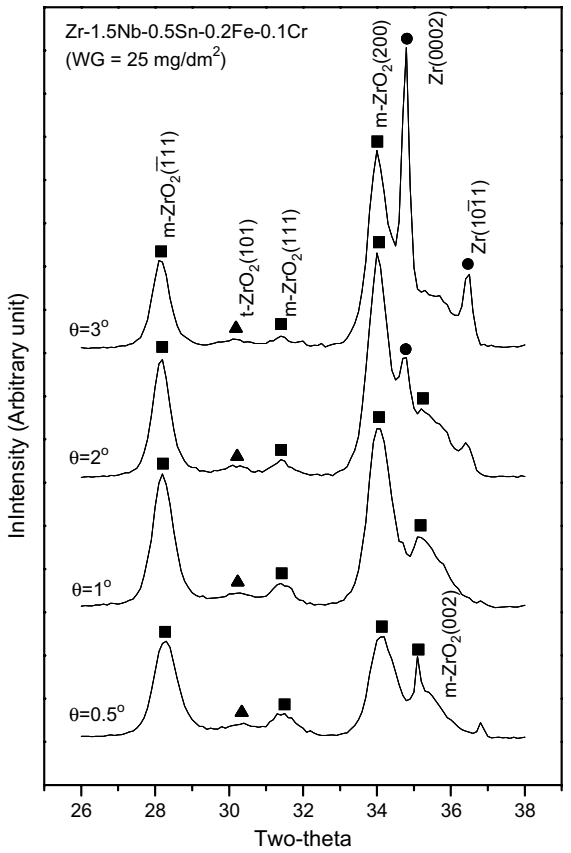

Fig. 7. Synchrotron X-ray diffraction patterns at the incident angles of 0.5°, 1°, 2° and 3° measured on the oxide of Zr–1.5Nb–0.5Sn–0.2Fe–0.1Cr which is intermediate-annealed at 575 °C for 8 h and corroded up to a weight gain of about 25 mg/dm^2.

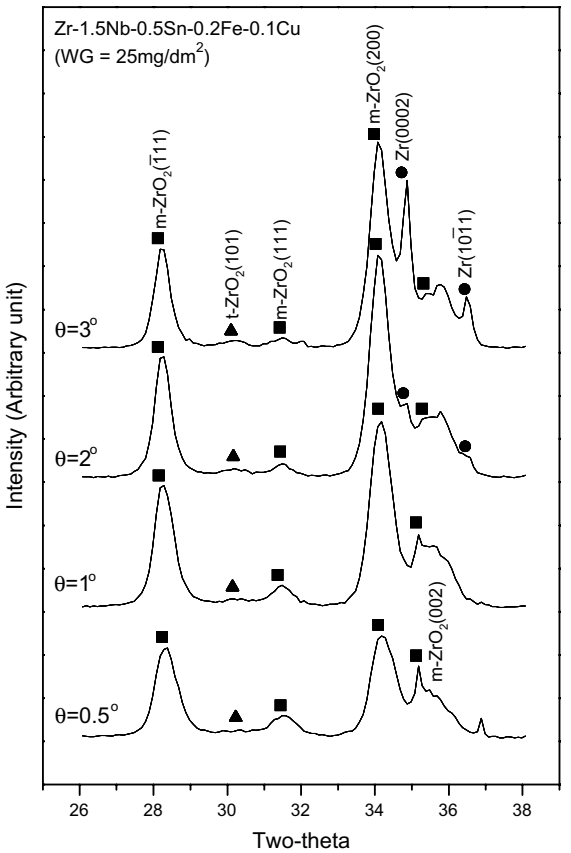

Fig. 8. Synchrotron X-ray diffraction patterns at the incident angles of 0.5°, 1°, 2° and 3° measured on the oxide of Zr–1.5Nb–0.5Sn–0.2Fe–0.1Cu which is intermediate-annealed at 575 °C for 8 h and corroded up to a weight gain of about 25 mg/dm^2.

ence of the phase fraction gradient. Although the ratio of the integrated intensity calculated in this investigation was not identical to the volume fraction of the tetragonal phase, it can be used to show a relative change of the crystal structure in the oxide [21,22]. As a result of this investigation, it could be clarified that the tetragonal phase fraction was a maximum near the metal/oxide interface and decreased when apart from the interface, and the corrosion resistance of the Zr alloys was improved in case that the tetragonal phase fraction was higher in the metal/oxide interface.

It was reported that the oxide layer with a higher fraction of the tetragonal phase was more protective to the oxidation [23]. The oxide is degraded in terms of the protectiveness to the oxidation when it moves from the interface to the surface region, though the protective layer is newly formed and maintained at the interface. The tetragonal phase fraction was higher at the protective layer near the interface than the outer surface region. This is caused by that one of the main reasons for stabilizing the tetragonal phase is the compressive stress induced by the transformation of Zr to ZrO_2. Thus, it would be suggested that the oxide layer with a higher fraction of the tetragonal phase has a protective nature to the oxidation although the tetragonal phase itself was not considered as the main reason for improving the protectiveness of the oxide. Therefore, the superior corrosion resistance of the Cu-containing alloy to the Cr-containing alloy is thought to be attributable to the lager amount of the tetragonal phase in the metal/oxide interface.

Fig. 10 shows the result of the glancing angle XRD on the Cu-containing alloys intermediate-annealed at 575 °C for 3 h, 8 h and 15 h. The incident angle was fixed at 3° for all three samples to analyze the region of the metal/oxide interface where there is an appreciable amount of the tetragonal zirconia. The fraction of the tetragonal phase is depicted as a function of the intermediate

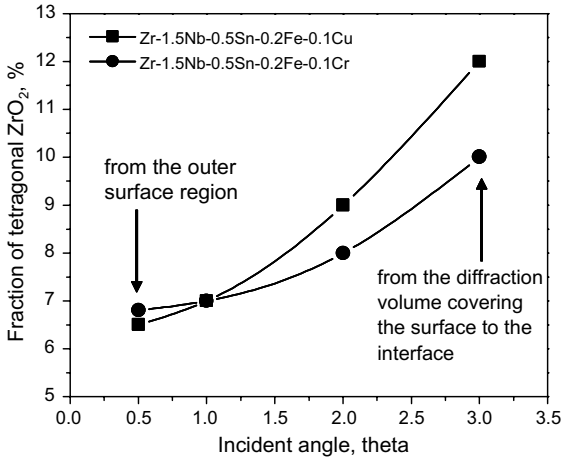

Fig. 9. The fraction of the tetragonal phase in the oxide as a function of the depth from the outer surface.

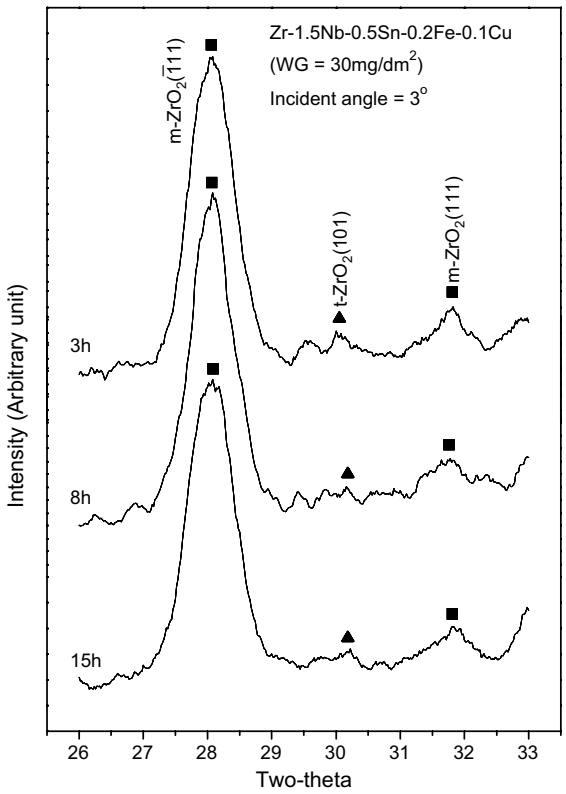

Fig. 10. Synchrotron X-ray diffraction patterns at the incident angle of 3° measured on the oxide of Zr–1.5Nb–0.5Sn–0.2Fe–0.1Cu which is intermediate-annealed at 575 °C for 3 h, 8 h and 15 h, and corroded up to a weight gain of about 30 mg/dm^2.

annealing time in Fig. 11. The corrosion resistance and the mean particle size of the Cu-containing alloys are

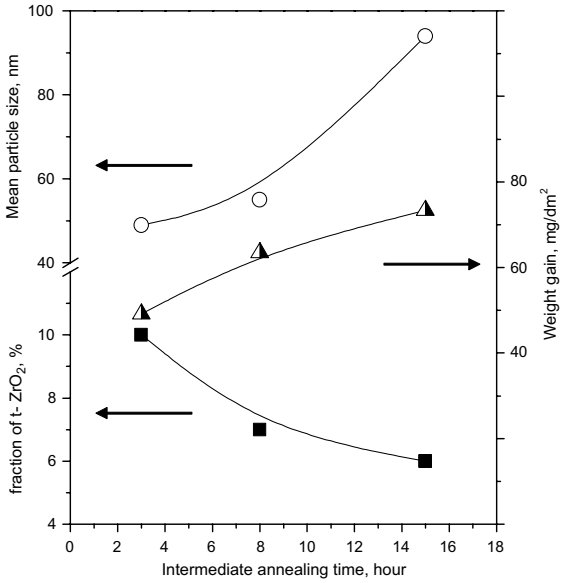

Fig. 11. The corrosion resistance, the mean particle size of the precipitates and the fraction of the tetragonal phase as a function of the intermediate annealing time in Zr–1.5Nb–0.5Sn–0.2Fe–0.1Cu.

also shown for comparison in Fig. 11. The three parameters would be closely related to each other. As shown in Fig. 2, when the intermediate annealing time increased, the corrosion resistance of the Cu-containing alloys decreased, which is accompanied by an increasing of the mean particle size and a decreasing of the tetragonal phase in the metal/oxide interface.

3.5. Effects of the precipitates on the stabilization of tetragonal ZrO_2

The mechanism of the stabilization of the tetragonal zirconia in the oxide is still under discussion and can be explained in several ways such as the high compressive stress in the oxide [23–25], the small grain size [21] or the presence of the point defect [26]. The tetragonal zirconia is stable at temperatures above 1150 °C, but it can be stabilized at lower temperatures in the presence of high compressive stresses. It is widely known that high compressive stresses are build up during oxidation due to a high Pilling–Bedworth ratio (1.56 for Zr). This stress is assumed to be responsible for the tetragonal phase stabilization by several authors [23–25]. It is also reported that the precipitates played a role in the generation of the additional stress in the oxide layer [23]. In this investigation, the corrosion behavior of Zr alloys was correlated with the precipitate characteristics by discussing the role of precipitates in the oxide. It is well known that the precipitates are able to enhance the cor-

rosion resistance of Zr alloys. The most probable reason why the Zr alloys containing precipitates showed a better corrosion resistance than the pure Zr is related to the delayed oxidation of the precipitates in the oxide, thereby extending the stability of the tetragonal phase by the additional stress build-up [27].

In general, the oxide of the Zr alloys was reported to consist of two layers according to the degree of the porosity. The dense oxide is formed in the interface region while the oxide in the outer surface region can be characterized as porous. It is known that the corrosion behavior of the Zr alloys is controlled by the dense oxide layer near the interface in which the fraction of the tetragonal phase is higher than the outer surface region. One of the main reasons for the stabilization of the tetragonal phase in the interface region is attributable to the compressive stress which is derived from the transformation of Zr alloys to Zr oxide by the oxidation process. In outer part of the oxide, however, the relaxation of the stress build-up arises in company with the destabilization of the tetragonal phase. It is noted here that the high compressive stress build-up means that there is no stress relaxation process such as crack initiation which usually leads to the loss of the protectiveness. Therefore, it seems that tetragonal phase fraction in the oxide can be regarded as one of the criteria for the protectiveness of the oxide though it is not clarified that the tetragonal phase itself has a protective nature to the oxidation.

Nevertheless, the corrosion resistance of Zr alloys could not be fully explained by the degree of the tetragonal phase fraction in the oxide in case that the alloy type was significantly different. It was reported that Zr–1Nb–O alloy showed a better corrosion resistance than Zircaloy-4 although the tetragonal phase fraction in the oxide was lower in Zr–1Nb–O alloy [28]. It means that the difference of corrosion resistance between the two alloys is not able to be clarified solely by the tetragonal phase stability. However, it is suggested that the tetragonal phase fraction can be considered as one of the criteria for the protectiveness of the oxide in the alloys with a similar compositions.

The precipitates are not oxidized at the same time as the surrounding metal in the oxidation process of Zr alloy, but incorporated into the oxide in unoxidized state. When the incorporated precipitates oxidize at a certain distance from the interface in the oxide, the additional stress is build up by the volume difference between the initial precipitate and the newly formed zirconia. This additional stress is thought to be effective to extend the stability of tetragonal phase in the oxide [27], thereby maintaining the protectiveness to a longer position from the metal/oxide interface. This behavior is thought to be largely dependant on the precipitate characteristics. The oxidation of β-Nb was found to be delayed more than the $Zr(Fe,Cr)_2$-type precipitates when they were incorporated into the oxide [29]. It would imply that the delayed oxidation of β-Nb is effective to extend the protectiveness to a longer position from the metal/oxide interface.

On the other hand, the number of precipitates per unit volume was considered to be the predominant metallurgical factor controlling the corrosion kinetics [30]. The distribution of the additional stress would be quite different in the oxide depending on the size distribution of precipitates although the amount of the additional stress build-up by the delayed oxidation of the precipitates depends only on the total volume fraction of the precipitates in the oxide. The distribution of the additional stress would be more homogeneous when the precipitates with a finer distribution are oxidized lately in the oxide as compared to the larger size precipitates with a coarse distribution. There might be an optimal level of the additional stress build-up above which the stress relaxation process such as crack propagation is operating, thereby degrading the protectiveness of the oxide. The large precipitate might enhance the stress concentration at a local region in the oxide when it is oxidized in the oxide as compared to the small precipitates. It is therefore suggested that the fine distribution of small precipitates is more desirable for the homogeneous distribution of the additional stress, thereby being more beneficial to the corrosion resistance.

In this study, the relative fraction of the fine precipitates, which are mostly identified by β-Nb, were higher in the Cu-containing alloy than the Cr-containing alloy when heat-treated in the same condition. Thus the stabilization of the tetragonal phase in the oxide is more promoted in the Cu-containing alloy than the Cr-containing alloys, as shown in Fig. 9, which could be the main reason for the superior corrosion resistance of the Cu-containing alloys to the Cr-containing alloy, as shown in Fig. 1. On the other hand, the stabilizing effect by the precipitates decreases when the particle size increases with increasing the intermediate annealing time. Based on the result, it could be concluded that the excellent corrosion resistance of Zr alloys with a high Nb content can be achieved by maintaining a uniform distribution of the fine second phase particles.

4. Conclusions

The corrosion behavior of Zr alloy with a high Nb content was evaluated in a water loop system containing 2.2 wppm Li and 650 wppm B. The corrosion test results showed that the Cu addition was of benefit to the corrosion resistance of Zr–1.5Nb–0.5Sn–0.2Fe and the corrosion resistance of the Cu-containing alloy (Zr–1.5Nb–0.5Sn–0.2Fe–0.1Cu) was superior to that of the Cr-containing alloy (Zr–1.5Nb–0.5Sn–0.2Fe–0.1Cr). It was shown that the corrosion behavior of the Cr- and

Cu-containing alloy was highly influenced by the precipitate characteristics, which were practically determined by the intermediate annealing after the hot rolling. The fine precipitates, which are mostly identified by β-Nb, were found more frequently in the Cu-containing alloy than the Cr-containing alloy when heat-treated in the same condition. The oxide formed in the corrosion test was characterized by an X-ray diffraction method using a synchrotron radiation. The ratio of the tetragonal phase in the region of the metal/oxide interface was higher in the Cu-containing alloy than the Cr-containing alloy. Thus the stabilization of the tetragonal phase in the oxide is promoted more when the mean particle size of the precipitates decreased, which could be the main reason for the superior corrosion resistance of the Cu-containing alloys to the Cr-containing alloy. It is concluded that a fine distribution of β-Nb is desirable for stabilizing the tetragonal phase by the additional stress in the oxide, thereby increasing the corrosion resistance of the Zr alloy with a high Nb content.

Acknowledgement

This work has been carried out under the nuclear R&D program by MOST in Korea. Experiments at PLS were supported in part by MOST and POSTECH.

References

[1] F. Garzarolli, H. Stehle, E. Steinberg, ASTM STP 1295 (1996) 12.
[2] G.P. Sabol, G.R. Kilp, M.G. Balfour, E. Roberts, ASTM STP 1023 (1989) 227.
[3] A.V. Nikulina, A.M. Vladimir, M.M. Peregud, Y.K. Bibilashvili, V.A. Kotrekhov, A.F. Lositsky, N.V. Kuzmenko, Y.P. Shevnin, V.K. Shamardin, G.P. Kobylyansky, A.E. Novoselov, ASTM STP 1295 (1996) 785.
[4] J.-P. Mardon, D. Charquet, J. Senevat, ASTM STP 1354 (2000) 505.
[5] K. Yamate, A. Oe, M. Hayashi, T. Okamoto, H. Anada, S. Hagi, in: Proceedings of the 1997 International Topical Meeting on LWR Fuel Performance, 1997. p. 318.
[6] G.P. Sabol, R.J. Comstock, R.A. Weiner, P. Larourer, R.N. Stanutz, ASTM STP 1245 (1994) 724.
[7] R.J. Comstock, G. Schoenberger, G.P. Sabol, ASTM STP 1295 (1996) 710.
[8] H. Anada, K. Nomoto, Y. Shida, ASTM STP 1245 (1994) 307.
[9] T. Isobe, Y. Matsuo, ASTM STP 1132 (1991) 346.
[10] J.Y. Park, Y.H. Jeong, Y.H. Jung, Met. Mater. Int. 7 (2001) 447.
[11] Y.H. Jeong, K.O. Lee, H.G. Kim, J. Nucl. Mater. 302 (2001) 9.
[12] Y.H. Jeong, H.G. Kim, D.H. Kim, J. Nucl. Mater. 317 (2003) 1.
[13] S.W. Ha, J.Y. Huh, J.Y. Park, Y.H. Jeong, J. Kor. Inst. Met. Mater. 39 (2001) 1092.
[14] H.S. Hong, J.S. Moon, S.J. Kim, K.S. Lee, J. Nucl. Mater. 297 (2001) 113.
[15] V.F. Urbanic, B.D. Warr, A. Manolescu, C.K. Chow, M.W. Shanahan, ASTM STP 1023 (1989) 20.
[16] V.F. Urbanic, R.W. Gilbert, in: Proceedings of IAEA Technical Committee Meeting on Fundamental Aspects of Corrosion on Zirconium Base Alloys in Water Reactor Environments, International Atomic Energy Agency, Vienna, IWGFPT/34, 1990, p. 262.
[17] G.P. Sabol, G. Schoenberger, M.G. Balfour, in: Proceedings of IAEA Technical Committee Meeting on Materials for Advanced Water Cooled Reactor, International Atomic Energy Agency, Vienna, IAEA-TECDOC-665, 1992, p. 122.
[18] Ch. Valot, D. Ciosmak, M.T. Mesnier, M. Lallemant, Oxid. Met. 48 (1997) 329.
[19] K.T. Erwin, O. Delaire, A.T. Motta, Y.S. Chu, D.C. Mancini, R.C. Birtcher, J. Nucl. Mater. 294 (2001) 299.
[20] R.C. Garvie, P.S. Nicholson, J. Am. Ceram. Soc. 55 (1972) 303.
[21] P. Barberis, J. Nucl. Mater. 226 (1995) 34.
[22] K. Takeda, H. Anada, ASTM STP 1354 (2000) 592.
[23] J. Godlewski, ASTM STP 1245 (1994) 663.
[24] J. Godlewski, J.P. Gros, M. Lanbertin, J.F. Wadier, H. Weidinger, ASTM STP 1132 (1991) 416.
[25] H.J. Beie, A. Mitwaslky, F. Gazarolli, H. Ruhmann, H.J. Sell, ASTM STP 1245 (1994) 615.
[26] M. Osendi, J.S. Moya, J. Am. Ceram. Soc. 68 (1985) 135.
[27] D. Pecheur, F. Lefebvre, A.T. Motta, C. Lemaignan, J.F. Wadier, J. Nucl. Mater. 189 (1992) 318.
[28] P. Bossis, J. Thomazet, F. Lefebvre, ASTM STP 1423 (2002) 190.
[29] D. Pecheur, J. Nucl. Mater. 278 (2000) 195.
[30] D. Charquet, J. Nucl. Mater. 288 (2001) 237.